

Original citation:

Janik, Vit, Lan, Yongjun, Beentjes, Peter, Norman, David, Hensen, Guido and Sridhar, Seetharaman. (2016) Zn diffusion and α -Fe(Zn) layer growth during annealing of Zn-coated B steel. Metallurgical and Materials Transactions A - Physical Metallurgy and Materials Science, 47 (1). pp. 400-411.

Permanent WRAP URL:

<http://wrap.warwick.ac.uk/75484>

Copyright and reuse:

The Warwick Research Archive Portal (WRAP) makes this work by researchers of the University of Warwick available open access under the following conditions. Copyright © and all moral rights to the version of the paper presented here belong to the individual author(s) and/or other copyright owners. To the extent reasonable and practicable the material made available in WRAP has been checked for eligibility before being made available.

Copies of full items can be used for personal research or study, educational, or not-for profit purposes without prior permission or charge. Provided that the authors, title and full bibliographic details are credited, a hyperlink and/or URL is given for the original metadata page and the content is not changed in any way.

Publisher's statement:

"The final publication is available at Springer via [http://dx.doi.org/\[insert DOI\]](http://dx.doi.org/[insert DOI])".

A note on versions:

The version presented here may differ from the published version or, version of record, if you wish to cite this item you are advised to consult the publisher's version. Please see the 'permanent WRAP URL' above for details on accessing the published version and note that access may require a subscription.

For more information, please contact the WRAP Team at: wrap@warwick.ac.uk

Zn Diffusion and α -Fe(Zn) Layer Growth During Annealing of Zn-Coated B Steel



VIT JANIK, YONGJUN LAN, PETER BEENTJES, DAVID NORMAN,
GUIDO HENSEN, and SEETHARAMAN SRIDHAR

Direct hot press forming of Zn-coated 22MnB5 steels is impeded by micro-cracks that occur in the substrate due to the presence of Zn during the forming process. A study was therefore undertaken to quantify concentration of Zn across the α -Fe(Zn) coating and on grain boundaries in the α -Fe(Zn) layer and the underlying γ -Fe(Zn) substrate after isothermal annealing of Zn-coated 22MnB5 at 1173 K (900 °C) and to link the Zn distribution to the amount and type of micro-cracks observed in deformed samples. Finite difference model was developed to describe Zn diffusion and the growth of the α -Fe(Zn) layer. The penetration of Zn into the γ -Fe(Zn) substrate after 600 seconds annealing at 1173 K (900 °C) through bulk diffusion is estimated to be 3 μ m, and the diffusion depth of Zn on the γ -Fe(Zn) grain boundaries is estimated to be 6 μ m, which is significantly shorter than the maximum length (15 to 50 μ m) of the micro-cracks formed in the severely stressed conditions, indicating that the Zn diffusion into the γ -Fe(Zn) from the α -Fe(Zn) during annealing is not correlated to the depth of micro-cracks. On the other hand, the maximum amount of Zn present in α -Fe(Zn) layer decreases with annealing time as the layer grows and Zn oxidizes, and the amount of Zn-enriched areas inside the α -Fe(Zn) layer is reduced leading to reduced length of cracking. Solid-Metal-Induced Embrittlement mechanism is proposed to explain the benefit of extended annealing on reduced depth of micro-crack penetration into the γ -Fe(Zn) substrate.

DOI: 10.1007/s11661-015-3203-y

© The Minerals, Metals & Materials Society and ASM International 2015

I. INTRODUCTION

THE automotive industry is facing increasing demands for improved passenger safety, environmental performance, and costs reduction.^[1] Ultra-high-strength steels (UHSS) were developed to offer substantial improvement of passive safety, thanks to their ultra-high strength of 1500 to 2000 MPa and simultaneously to allow manufacturing of critical parts (A-, B-pillars, roof rails, crash management structures) *via* direct hot press forming process (HPF) to enable forming of complex light weight components at high volumes and low costs.^[2] To meet requirement on corrosion resistance, UHSS are usually supplied coated either with an Al-Si coating that offers passive corrosion resistance or with a Zn-based coating that provides active cathodic protection.^[3,4]

In the direct HPF process, a coated blank is austenitized and subsequently formed and quenched in a single

press stroke to achieve the desired strength. However, Zn-coated 22MnB5 steels when exposed to temperatures of 1153 K to 1203 K (880 °C to 930 °C) during the HPF are known to suffer from different types of cracking.^[3,5] The mechanism of cracking in Zn-coated steel is believed to be a combination of (a) cracks initiated inside the coating as a result of different coefficient of thermal expansion of the coating and the substrate^[4]; (b) mechanical micro-cracks either newly nucleated on the surface or advancing from already cracked coating layer under the influence of friction^[3]; (c) liquid-metal-induced embrittlement (LMIE) due to the presence of liquid Zn in the coating,^[6-8] and (d) embrittlement induced by enrichment of Zn on γ -Fe(Zn) grain boundaries during the annealing stage prior to HPF.^[9]

It is well understood that the Zn-based coating undergoes a series of phase transformations driven by diffusion of Fe into the coating during heating stage before HPF^[10]: initial soft Zn-rich η -phase (almost pure Zn) is transformed into hard Γ and Γ_1 phases (17 to 19.5 and 23.5 to 28.0 wt pct Fe, respectively). Equilibrium phase diagram for 22MnB5 has been calculated using FactSage to give guidance about the phases present at the temperature of HPF (Figure 1). Phase transformations and reactions are accompanied on the coating surface by turbulences of the coated layer at temperatures between 773 K and 1073 K (500 °C and 800 °C) with severe outbursts of Zn occurring on the interface between the coating and the substrate, and by formation of locations with accumulated Zn and possibly increased

VIT JANIK, Research Fellow, and SEETHARAMAN SRIDHAR, Professor, are with the WMG, University of Warwick, Coventry CV4 7AL, U.K. Contact e-mail: v.janik@warwick.ac.uk YONGJUN LAN, Principal Researcher, is with the Swinden Technology Centre, Tata Steel, R&D, Moorgate Road, Rotherham S60 3AR, U.K. PETER BEENTJES and GUIDO HENSEN, Principal Researchers, are with the IJmuiden Technology Centre, Tata Steel, R&D, 1970 CA IJmuiden, The Netherlands. DAVID NORMAN, Principal Researcher, is with the Automotive Engineering Group, Tata Steel, R&D, Coventry CV4 7AL, U.K.

Manuscript submitted December 11, 2014.



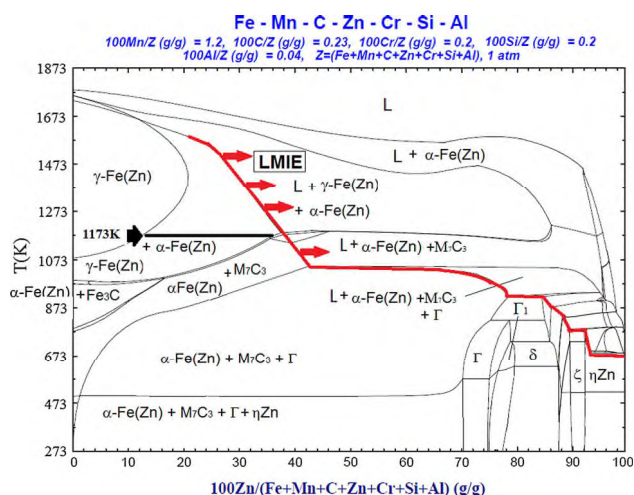


Fig. 1—Phase diagram of Fe-C-Al-Mn-Cr-Si-Zn system calculated by FactSage.

Zn content.^[10] Additionally, the surface layer of the coating is oxidized at the annealing temperatures with complex and morphologically heterogeneous oxide layer (OL) formed.^[11] Finally, given enough time at temperatures above 1123 K (850 °C), the coating will be largely transformed into a solid solution of Zn in α -Fe(Zn) that with extended stay at the forming temperature will grow in thickness.^[3,5,12]

It has been observed that no liquid Zn is present neither in the coating nor in the steel substrate at the annealing temperature above 1173 K (900 °C) if annealing treatment ranging from 180 to 720 seconds in duration is applied prior to the HPF process.^[3,4,6,9–11] In this case, LMIE is completely avoided. However, the maximum depth of the micro-cracks is still 30 to 50 μ m into the substrate for severe forming conditions if a short annealing time (between 240 and 300 seconds) is applied. If annealing time at 1173 K (900 °C) is increased to more than 500 seconds, the depth of the cracking is limited to 10 to 15 μ m,^[12] this is close to the crack depth (less than 10 μ m) acceptable for the automotive industry.^[9] However, the exact mechanisms responsible for the reduced micro-crack penetration into the γ -Fe(Zn) substrate with extended annealing together with the role of Zn distribution across the coating and in the substrate are not yet fully understood.^[12]

The objective of this work is to assess the extent to which Zn diffusion occurs into the γ -Fe(Zn) austenite phase during the annealing process prior to forming and whether this can be correlated to the penetration depth of cracks in the γ -Fe(Zn) substrate. The approach is through scanning (SEM) and transmission electron microscopy (TEM), and energy-dispersive spectroscopy (EDS) characterization of the Zn distribution of samples annealed between 240 and 600 seconds prior to HPF at 1173 K (900 °C) in combination with the development of a finite difference model (FDM) to describe Zn diffusion and the growth of the α -Fe(Zn) during isothermal annealing of Zn-coated 22MnB5.

II. MATERIALS AND METHODS

A. Experimental Material and Metallography

The material used in this study was Zn-coated 22MnB5 steel with a coating weight of approximately 130 g/m² provided by Tata Steel. The total strip thickness was 1.65 mm. Strips of this material were placed in a roller hearth furnace with air atmosphere heated to 1173 K (900 °C) prior to HPF for 240, 300, 480, and 600 seconds, respectively. The experimental stamping process was applied after different isothermal holding times to form U-shaped profiles with drawing depth of 50 mm, draw gap and spacer distance of 0.15 mm, die radius of 2 mm, and forming speed of 300 mm/s.^[12]

Metallographic samples were taken from a non-deformed top and from a severely drawn side that is exposed to friction forces during stamping; for details on the experimental procedure and results, please see.^[12] Standard metallographic methods for sample preparation were applied; the final etching step depended on the type of analysis performed: (i) non-etched for SEM back scattered electron imaging (BSEI) and EDS data collection (mapping, line scans, and point analysis); (ii) etched in saturated solution of picric acid in ethanol and wetting agent at 348 K (75 °C) to reveal prior austenite grain boundaries; and (iii) etched in 1 pct picral followed by 1 pct nital for optical microscopy (OM) and SEM secondary electron imaging (SEI) to analyze the coating/substrate interface, development of the coating thickness and the coating grain size. OM Zeiss Axio Scope A1 and Field Emission Gun SEM Carl Zeiss Gemini with EDS were used. FIB lift-out method at JEOL 4500 focused ion beam (FIB) SEM was applied on polished cross sections to prepare sections for further TEM analysis. First, locality on the coating/substrate interface containing α -Fe(Zn) grains and prior austenite grain was protected by a C layer to prevent ion milling of the surface, then cross-section lift-out samples and in-plane sections of area about 10 \times 10 μ m were taken out and attached to a Cu grid, and finally, FIB ion thinning was applied to prepare 100 nm thin foils for TEM. JEOL 2000FX and JEOL 2100 with EDS operating at 200 kV were used to analyze the FIB cross- and in-plane sections. Additional elemental line scans and mapping were performed by JEOL 2100 operating in scanning (STEM) mode with spot size of 5.5 nm.

B. Diffusion Model, Assumption, and Conditions

As shown by Marder^[10] during heating from the room temperature to approximately 1073 K (800 °C), complex phase transformations characterized by unstable transformation front and non-equilibrium thermodynamics involving various Zn-Fe intermetallic phases take place, making it extremely difficult to experimentally validate numerical models in this temperature range. 1173 K (900 °C), Zn-Fe intermetallic phases are not thermodynamically stable and only α -Fe(Zn) would be stable together with γ -Fe(Zn) (Figure 1). It has been reported^[10] that indeed after

173 180 seconds dwell at 1173 K (900 °C), the intermetallic
174 phases are fully transformed into α -Fe(Zn) and that Zn
175 diffuses from the α -Fe(Zn) phase into the austenite
176 phase of steel substrate to form γ -Fe(Zn). In addition to
177 diffusion and depending on the composition of the
178 coating and the furnace dew point, varying amount of
179 active metallic Zn in the coating is lost due to oxidation
180 in the air furnace atmosphere. About 2.0- μ m-thick ZnO
181 layer was observed on the outermost surface during the
182 heating and following isothermal dwell^[12] resulting in
183 approximately 70 pct of initial Zn to be available for
184 corrosion protection after the heat treatment is finished.
185 Therefore, after 180 seconds dwell at 1173 K (900 °C),
186 three layer structure is found with the innermost being
187 γ -Fe(Zn) austenitic substrate (austenite is transformed
188 into martensite after die quenching from HPF), the
189 middle α -Fe(Zn) coating, and the outermost oxide
190 ZnO.^[12] Since only three phases are present and
191 thermodynamically stable during the isothermal anneal-
192 ing (Figure 1), the isothermal stage is therefore chosen
193 to be simulated in this work.
194 The diffusion of Zn within α -Fe(Zn) layer and
195 γ -Fe(Zn) substrate at 1173 K (900 °C) is schematically
196 shown in Figure 2 with the substrate on the left, the
197 α -Fe(Zn) coating layer in the middle, and the Zn oxide
198 on the right side. During annealing, Zn diffuses from the
199 interface S_2 into the γ -Fe(Zn) substrate through the
200 α -Fe(Zn) layer. The speed of the interface S_1 is calcu-
201 lated using the Stefan condition as

$$v|_{x=S_1} = \left(D_{Zn}^{\gamma} \frac{\partial C_{Zn}^{\gamma}}{\partial x} - D_{Zn}^{\alpha} \frac{\partial C_{Zn}^{\alpha}}{\partial x} \right) / \left(C_{Zn}^{\alpha/\gamma} - C_{Zn}^{\gamma/\alpha} \right) \quad [1]$$

203 with D_{Zn}^{γ} , D_{Zn}^{α} effective diffusion coefficients in the
204 γ -Fe(Zn) substrate and the α -Fe(Zn) layer, C_{Zn}^{γ} , C_{Zn}^{α}
205 concentrations of Zn in these two phases, $C_{Zn}^{\alpha/\gamma}$, $C_{Zn}^{\gamma/\alpha}$
206 equilibrium concentrations at both sides of the α - γ

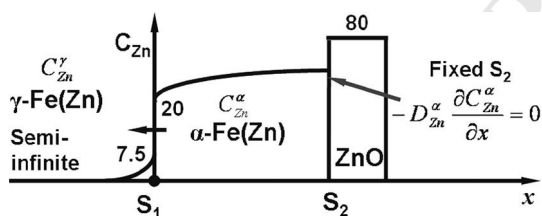


Fig. 2—1D model of Zn diffusion at 1173 K (900 °C) with S_2 fixed and no Zn flux across S_2 . The equilibrium Zn concentrations (20 and 7.5 wt pct) at both sides of S_1 are also given.

interface S_1 . On the right-hand side of Eq. [1], the con-
centration gradients $\frac{\partial C_{Zn}^{\gamma}}{\partial x}$, $\frac{\partial C_{Zn}^{\alpha}}{\partial x}$ within the γ -Fe(Zn) and
 α -Fe(Zn) phase interiors are controlled by the Fick's
second law, as shown below

$$\frac{\partial C}{\partial t} = D \frac{\partial^2 C}{\partial x^2}, \quad [2]$$

where C and D are Zn concentration and effective
diffusion coefficient either in the γ -Fe(Zn) substrate or in
the α -Fe(Zn) coating layer, t is time, and x is space
coordinate.

One-dimensional (1D) implicit finite difference
method (FDM) was developed to solve Eq. [2] together
with the moving boundary condition (Eq. [1]) for
calculating Zn concentration within the α -Fe(Zn) coat-
ing layer and the γ -Fe(Zn) substrate during annealing.
Figure 3 shows the starting Zn concentration used in the
1D FDM, which is mapped using the measured data
(EDS line scan) for annealing at 1173 K (900 °C) for
240 seconds furnace time. The initial average thickness
of the α -Fe(Zn) coating layer in the model is 17.8 μ m
taken from Table I. The 1D FDM is then used to
calculate Zn concentration in the α -Fe(Zn) coating layer
and the γ substrate annealed for 300, 480, and 600 sec-
onds at this temperature. The calculated concentration
profiles and α -Fe(Zn) layer thickness are compared to
the corresponding measured values, by which the
effective diffusivities of Zn in the α -Fe(Zn) coating and
the γ -Fe(Zn) substrate are calibrated since no data are
available for the effective diffusion coefficients in the
literature.

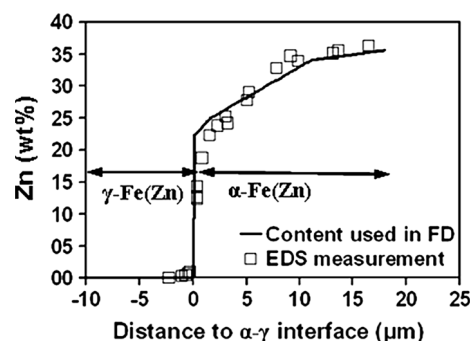


Fig. 3—Zn concentration profile used in the 1D FDM (solid line) as start condition of simulation. These model data are mapped using the values of EDS line scan (squares) for the annealing at 1173 K (900 °C) for 240 s. The thickness (17.8 μ m) of α -Fe(Zn) layer in the model is determined using the average value of measured thickness.

Table I. Average Depth of OL and of α Fe(Zn) Layer for All Heating Conditions at 1173 K (900 °C)

Time (s)	Avg. Thickness of OL (μ m)	Avg. Depth α Fe(Zn) (μ m)	Avg. Size of Columnar α Fe(Zn) Grains (μ m)		Avg. Size of Prior Austenite (γ -Fe(Zn)) Grain (μ m)
			Avg. Length (μ m)	Avg. Diameter (μ m)	
240	2.1 \pm 0.9	17.8 \pm 3.9	10.9 \pm 4.8	7.4 \pm 4.5	9.7 \pm 1.7
300	2.2 \pm 1.0	18.7 \pm 3.4	10.7 \pm 4.8	7.0 \pm 2.8	9.6 \pm 2.8
480	2.2 \pm 1.2	20.7 \pm 3.7	11.9 \pm 3.5	7.4 \pm 4.7	8.1 \pm 3.1
600	2.8 \pm 1.6	21.1 \pm 2.9	10.6 \pm 4.8	6.1 \pm 4.8	8.6 \pm 3.2

236 In the FDM, the following assumptions are made on
 237 the boundary conditions and the diffusion coefficients:

- 238 • the interface S_2 is planar and stationary, and the Zn
 239 diffusion flux across S_2 is equal to zero because the
 240 measured weight change showing only a thin layer of
 241 coating (about $2.0\text{-}\mu\text{m}$ thick) is oxidized during the
 242 annealing time from 240 to 600 seconds and that the
 243 oxidation kinetics is approximately linear;
- 244 • the interface S_1 is also planar and the boundary
 245 conditions are determined using Eq. [1];
- 246 • Zn diffusion coefficients in the $\alpha\text{-Fe(Zn)}$ layer and in
 247 the $\gamma\text{-Fe(Zn)}$ substrate are independent of Zn con-
 248 tents in these two phases and are taken thus as
 249 constants; and
- 250 • for diffusion coefficient calibration, the published
 251 lattice diffusivity of Zn in the $\alpha\text{-Fe(Zn)}$ layer^[13] is
 252 used in the reaction layer; however, since no data for
 253 the diffusivity of Zn in the $\gamma\text{-Fe(Zn)}$ substrate are
 254 reported in the literature, the lattice diffusion coef-
 255 ficient of Fe in $\gamma\text{-Fe}$ ^[14] is used.

256 Space step size $0.1\text{ }\mu\text{m}$ and time step size 0.001 second
 257 are used in all the calculations.

258 III. RESULTS

259 A. Morphology of the Coating

260 Figure 4(a) shows the near-surface micro-structure of
 261 the top undeformed wall of the U-shaped profile
 262 obtained in unetched condition by BSEI-SEM after
 263 heating at 1173 K ($900\text{ }^\circ\text{C}$) for 240 seconds. This
 264 section, unlike the side walls of the final U-shape profile,
 265 was not exposed to friction and did not receive any
 266 drawing during HPF either. The micrograph demon-
 267 strates three different regions present inside the coating:
 268 the top OL of 1 to $3\text{ }\mu\text{m}$ in thickness, $\alpha\text{-Fe(Zn)}$ layer is in
 269 the middle, and the martensitic substrate (m) at the
 270 bottom. It is apparent that the coating is cracked but the
 271 cracks do not penetrate into the martensitic substrate.
 272 Since top wall was not in contact with the die and not
 273 drawn, these cracks might be formed during quenching

274 after forming due to the difference of thermal expansion
 275 between the coating and the substrate. Elemental maps
 276 of Zn by SEM-EDS are shown from the coating, the
 277 interface as well as the substrate in Figures 4(b) and (c).
 278 At short annealing time, it is clearly visible that the
 279 $\alpha\text{-Fe(Zn)}$ /substrate interface is “wavy” with occurrence
 280 of waves corresponding to the grain boundaries separ-
 281 ating $\alpha\text{-Fe(Zn)}$ grains. With increasing annealing time,
 282 the wavy interface becomes less apparent. Table I
 283 summarizes measurements of the average thickness of
 284 the OL, depth of the $\alpha\text{-Fe(Zn)}$ layer, average size of the
 285 columnar $\alpha\text{-Fe(Zn)}$ grains, and of the prior austenite
 286 ($\gamma\text{-Fe(Zn)}$) grain size. Apart from the growth of the
 287 thickness of $\alpha\text{-Fe(Zn)}$ layer and of the OL, all other
 288 microstructural parameters are not greatly influenced by
 289 increased annealing time—differences are lower than the
 290 standard deviation which is large due to coating
 291 heterogeneities such as Zn outbursts occurring earlier
 292 during turbulent events at the heating stage.^[10]

293 Further details of the interface morphology at
 294 240 seconds are provided in Figure 5(a) taken by SEI.
 295 Faceted interface is apparent coinciding with $\alpha\text{-Fe(Zn)}$
 296 grain boundaries. Zn EDS map in Figure 5(b) shows
 297 possible Zn-rich pocket associated with $\alpha\text{-Fe(Zn)}$ grain
 298 boundary and possible location of previous Zn-rich
 299 Γ -phase^[6]; Figure 5(c) shows EDS Zn line scan across
 300 the $\alpha\text{-Fe(Zn)}$ grain boundary with increased Zn in the
 301 vicinity of the grain boundaries. At longer annealing
 302 times, Zn enrichment was not detected by SEM-EDS.

303 B. Zn Distribution in the Coating, Substrate, and at the 304 Interface

305 To be able to measure the Zn concentration both
 306 inside the $\alpha\text{-Fe(Zn)}$, inside the substrate, and at the
 307 $\alpha\text{-Fe(Zn)}$ /substrate interface, both SEM and high-reso-
 308 lution STEM-EDS lines scans were performed.
 309 Figure 6(a) shows area selected prior to the in-plane
 310 FIB lift-out, with grain boundary between the $\alpha\text{-Fe(Zn)}$
 311 grains and boundary between the $\alpha\text{-Fe(Zn)}$ and the
 312 substrate all visible. Corresponding TEM bright-field
 313 image is shown in Figure 6(b), and the STEM-EDS Zn

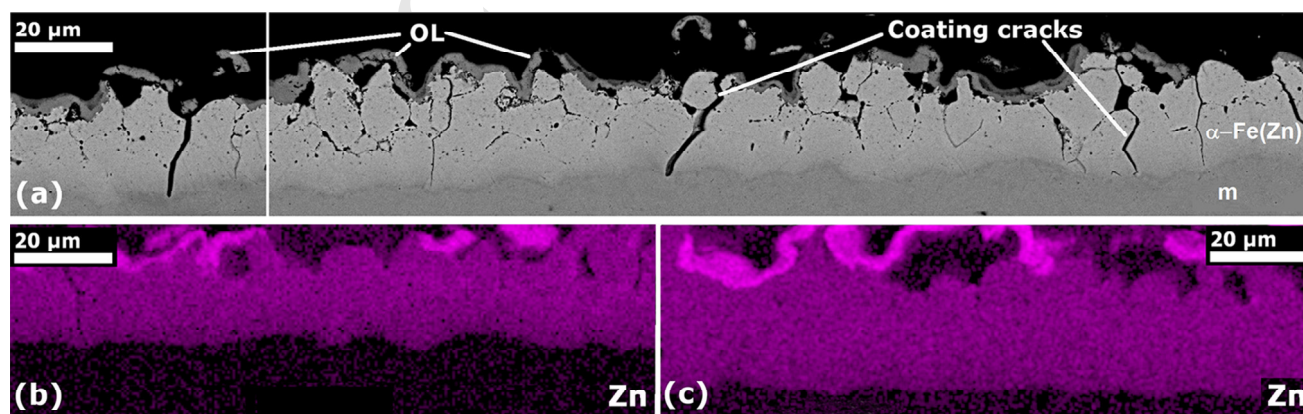


Fig. 4—(a) Unetched coating micrograph showing OL, $\alpha\text{-Fe(Zn)}$, and substrate (m) by BSEI SEM. Holding time 240 s at temperature 1173 K ($900\text{ }^\circ\text{C}$); (b) EDS Zn distribution map obtained at holding time 240 s at temperature 1173 K ($900\text{ }^\circ\text{C}$); (c) EDS Zn distribution map obtained at holding time 600 s at temperature 1173 K ($900\text{ }^\circ\text{C}$) showing less wavy interface between the $\alpha\text{-Fe(Zn)}$ layer and the substrate.

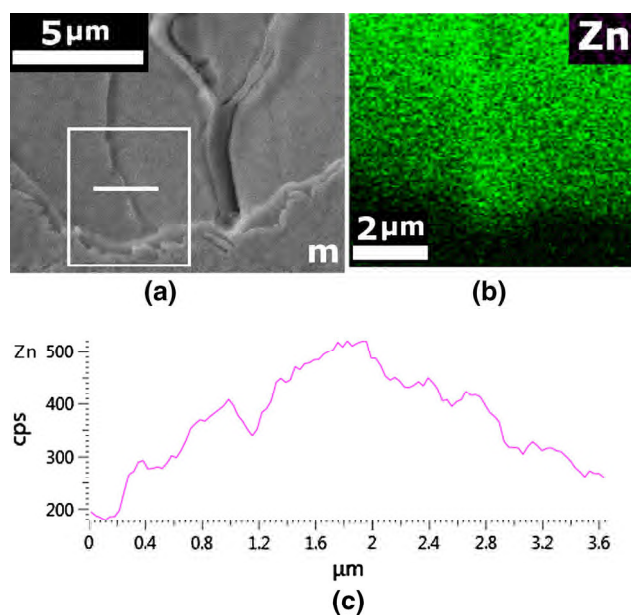


Fig. 5—(a) Detailed SEI micrograph of the α -Fe(Zn) grain boundary region etched in nital obtained after holding time 240 s at temperature 1173 K (900 °C); white rectangle and line indicate areas where EDS Zn map (b) and line scan (c) have been taken; m denotes the martensitic substrate with α -Fe(Zn) layer above.

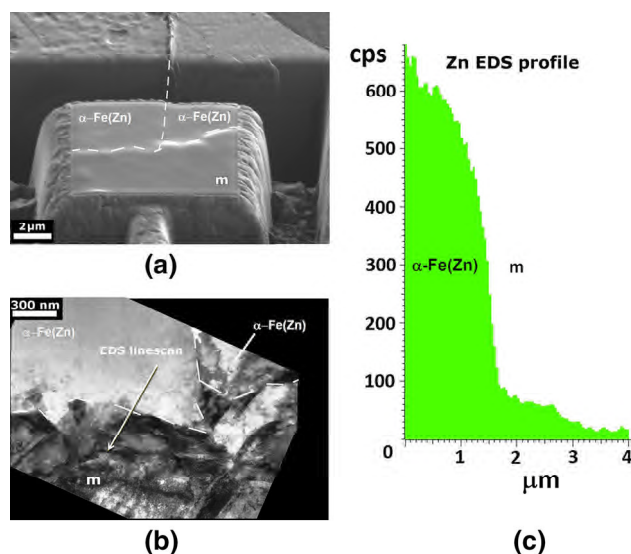


Fig. 6—(a) FIB SEM dual beam image showing location of the in-plane lift-out sample for TEM; in-plane lift-out locality is protected by a C layer applied onto its surface and is slightly obstructing the etched microstructural features; approximate location of GBs is visualized by dashed white lines; (b) TEM bright-field image of the lift-out area, yellow solid line indicates location where HR-TEM EDS line scan was performed; (c) Zn line scan from the interface region as collected by EDS; m denotes the martensitic substrate.

line scan is shown in Figure 6(c). Scanning STEM-EDS Zn profile shows sharp drop in the Zn concentration across the α -Fe(Zn)/substrate boundary which is observed across length of less than 700 nm.

Zn profiles measured by STEM and FEG-SEM EDS for all heating conditions are summarized in Figure 7.

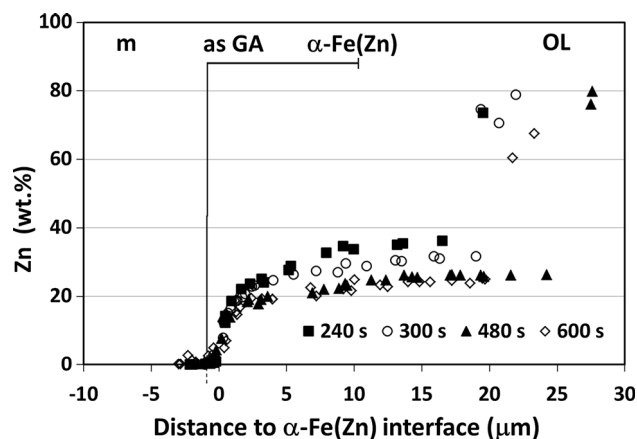


Fig. 7—Zn distribution profiles acquired by SEM and TEM EDS for all annealing conditions; dashed line shows initial as hot dip galvanized Zn profile.

Measured concentrations C_{Zn}^{α} of Zn in the bulk of α -Fe(Zn) near the top of the coating, C_{Zn}^{γ} of Zn in γ -Fe(Zn), and concentrations $C_{Zn}^{\alpha/\gamma}$, $C_{Zn}^{\gamma/\alpha}$ at both sides of the α - γ interface are presented in Table II.

C. Calculated Zn Concentration Profiles

Table III shows the equilibrium concentrations of Zn at both sides of the α - γ interface S_1 used in the calculations together with the calibrated effective diffusion coefficients in the α -Fe(Zn) coating and the γ -Fe(Zn) substrate. Details of the calibration process are given later in the Section IV-A.

Figure 8 shows the calculated Zn concentration profiles across the α -Fe(Zn) and γ -Fe(Zn) phases using the FDM as well as the corresponding values measured by EDS (obtained from Figure 7). It should be noted that the α - γ interface in Figures 8(a) through (c) is placed at the coordinate origin in order to compare the concentration around this interface. In the FDM, this interface S_1 moves into the γ -Fe(Zn) substrate. Results show good agreement between the calculation and the measurement for the Zn concentration (Figures 8(a) through (c)) and reasonable agreement for the α layer thickness (Figure 8(d)) if the diffusion coefficients are set to be the calibrated values: $D_{Zn}^{\alpha} = 5.00 \times 10^{-13}$ and $D_{Zn}^{\gamma} = 1.13 \times 10^{-14} \text{ m}^2 \text{ s}^{-1}$. The α -Fe(Zn) thickness after 480 and 600 seconds of annealing is about 2.0- μm thicker in the FDM than in the measurement because the oxidation of α -Fe(Zn) coating layer from 240 to 600 seconds is not considered in the model, as described before.

Results in Figure 8 show that Zn concentration in the α -Fe(Zn) layer decreases with annealing time, but both the Zn concentration and the diffusion distance in the γ -Fe(Zn) substrate increase with annealing time. It can also be seen that the thickness of α -Fe(Zn) coating layer increases from 240 to 600 seconds.

The good agreement between the calculated and the measured Zn concentrations at the distance 20 to 25 μm to the α - γ interface in Figures 8(a) through (c) implies that the boundary conditions (zero diffusion flux) set at

Table II. Experimentally Obtained Approximate Zn Concentrations in the Substrate and in the Coating

Annealing Time (s)	Measured Zn Concentration in Martensite/ γ -Fe(Zn) at Annealing Temperature (wt pct)		Measured Zn Concentration in α -Fe(Zn) (wt pct)	
	C_{Zn}^{γ}	$C_{Zn}^{\gamma/\alpha}$	C_{Zn}^{α}	$C_{Zn}^{\alpha/\gamma}$
240	<0.1	~1.5	35	<15
300	<0.1	~1.5	30	<15
480	<0.1	~1.5	25	<15
600	<0.1	~1.5	22	<15

Table III. Model Parameters Used in Eq. [1]

1173 K (900 °C)	Effective Zn Diffusion Coefficient ($m^2 s^{-1}$)	Equilibrium Zn Concentration (Wt Pct)
α -Fe(Zn)	5.00×10^{-13}	20
γ -Fe(Zn)	1.13×10^{-14}	7.5

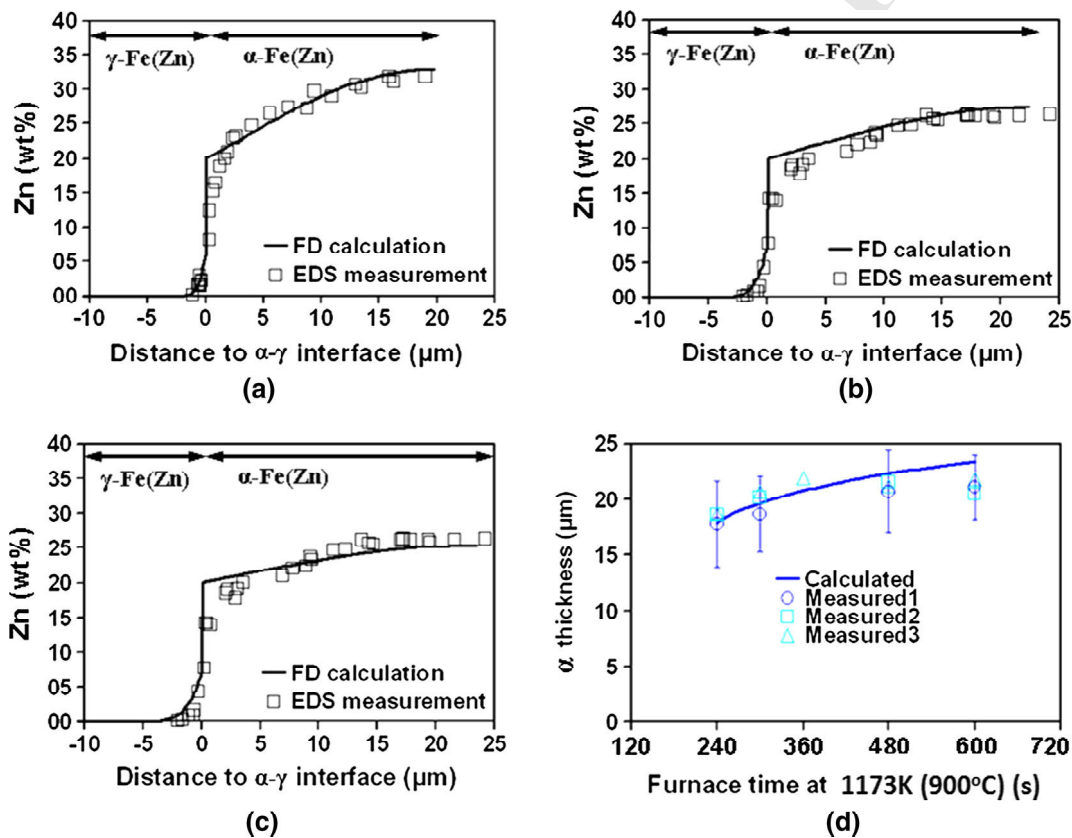


Fig. 8—Calculated Zn concentration profiles for different annealing times: (a) 300 s, (b) 480 s, and (c) 600 s and calculated α -Fe(Zn) layer thickness (d). Measured Zn concentration using EDS and measured α -Fe(Zn) layer thickness are also given for comparison.

the oxide- α -Fe(Zn) interface S_2 are reasonable. Both calculated and measured Zn concentrations are not lower at the oxide/ α -Fe(Zn) interface S_2 than at other locations within the α -Fe(Zn) coating layer. These results indicate that the depletion of Zn in the α -Fe(Zn) coating layer due to oxidation is relatively low for

annealing times of 240 to 600 seconds at 1173 K (900 °C).

It is shown in Figures 8(a) through (c) that the calculated and the measured Zn concentrations at the distance 10 to 25 μm to the α - γ interface decrease from about 31 wt pct for 300 seconds annealing to about

25 wt pct for 480 seconds annealing, but they remain to 25 wt pct approximately from 480 to 600 seconds, which means that the equilibrium concentration at the α side of α - γ interface is close to the value (20 wt pct) used in the calculation. Otherwise Zn concentration in the α -Fe(Zn) coating layer would decrease during the time period from 480 to 600 seconds.

The calculated and the measured Zn concentrations in the γ -Fe(Zn) substrate at the distance -5 to 0 μm to the α - γ interface are also in good agreement. This comparison suggests that the equilibrium concentration of Zn at the γ side of α - γ interface is about 7.5 wt pct, as used in the calculation.

The results shown in Figures 8(a) through (c) indicate that for the conditions examined, Zn in the α -Fe(Zn) coating layer diffuses primarily from the oxide- α -Fe(Zn) interface S_2 to the α - γ interface S_1 then further into the γ -Fe(Zn) substrate. Oxidation is found to slow down to an extent that Zn is not extracted out of the α -Fe(Zn) at a significant amount to supply the needed Zn for oxidation. The diffusion flux out of the α -Fe(Zn) into the γ -Fe(Zn) substrate does result in a decrease of the Zn concentration in the coating layer until it drops to the equilibrium concentration (20 wt pct) at the α - γ interface. On the other hand, the diffusion flux increases the concentration within the γ -Fe(Zn) substrate. The depth of Zn penetration into the γ -Fe(Zn) due to bulk

diffusion is calculated to be about 1.3 μm after 300 seconds annealing and it increases to about 2.6 and 3.3 μm after 480 and 600 seconds annealing, respectively.

IV. DISCUSSION

A. Choice of D

In order to calibrate the effective diffusion coefficients of Zn in the α -Fe(Zn) coating layer and in the γ -Fe(Zn) substrate, four 1D FDM simulations are carried out by changing the values for D_{Zn}^{α} and D_{Zn}^{γ} . Figure 9 shows the sensitivity of Zn concentration profiles and α -Fe(Zn) layer thickness on diffusion coefficients. If the diffusion coefficient D_{Zn}^{α} is increased from 1.11×10^{-14} to $5.00 \times 10^{-13} \text{ m}^2 \text{ s}^{-1}$ while maintaining $D_{\text{Zn}}^{\gamma} = 1.13 \times 10^{-17} \text{ m}^2 \text{ s}^{-1}$ fixed, the Zn concentration in the α -Fe(Zn) layer becomes lower, but the concentration in the γ -Fe(Zn) phase remains unchanged with an obvious increase observed in the α -Fe(Zn) layer thickness. When the diffusion coefficient D_{Zn}^{γ} increases from 1.13×10^{-17} to 1.13×10^{-13} through $1.13 \times 10^{-14} \text{ m}^2 \text{ s}^{-1}$ with $D_{\text{Zn}}^{\alpha} = 5.00 \times 10^{-13} \text{ m}^2 \text{ s}^{-1}$ fixed, Zn concentration in the γ -Fe(Zn) substrate increases significantly, but the value in the α -Fe(Zn) layer remains almost unchanged with an apparent decrease seen in the α -Fe(Zn) layer thickness.

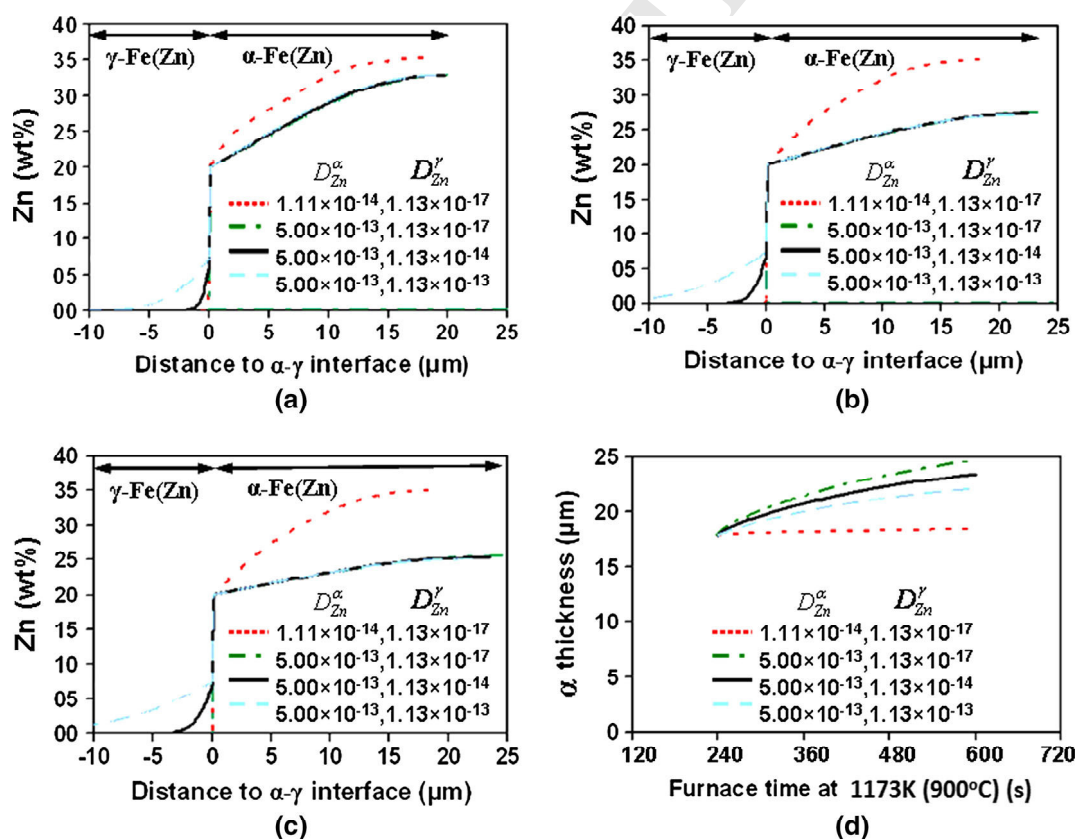


Fig. 9—Effect of D_{Zn}^{α} , D_{Zn}^{γ} on calculated Zn concentration profiles: (a) 300 s, (b) 480 s, and (c) 600 s and on calculated α -Fe(Zn) layer thickness (d).

Table IV. Comparison of Calibrated and Reported Diffusion Coefficients ($\text{m}^2 \text{s}^{-1}$)

1173 K (900 °C)	$\alpha\text{-Fe(Zn)}$	$\gamma\text{-Fe(Zn)}$
D_{Eff} (calibrated)	5.00×10^{-13}	1.13×10^{-14}
D_{L}	1.11×10^{-14} ^[13]	1.13×10^{-17} ^[14] (Fe in $\gamma\text{-Fe}$)
D_{gb}	2.08×10^{-10} ^[15]	1.29×10^{-12} ^[14] (Fe in $\gamma\text{-Fe}$)

Table V. Ratios of Diffusion Coefficients ($\text{m}^2 \text{s}^{-1}$) Between α and γ Phases

1173 K (900 °C)	D^{α}/D^{γ}
Zn (calibrated)	$5.00 \times 10^{-13}/1.13 \times 10^{-14} \approx 44$
C ^[14]	$1.70 \times 10^{-10}/5.90 \times 10^{-12} \approx 29$
Fe ^[14]	$1.86 \times 10^{-15}/1.13 \times 10^{-17} \approx 165$

The calculated Zn concentration profiles both in the $\alpha\text{-Fe(Zn)}$ layer and in the $\gamma\text{-Fe(Zn)}$ substrate using $D_{\text{Zn}}^{\alpha} = 5.00 \times 10^{-13}$ and $D_{\text{Zn}}^{\gamma} = 1.13 \times 10^{-14} \text{ m}^2 \text{s}^{-1}$ are in good agreement with the corresponding measured profiles, as shown in Figures 8(a) through (c). The calculated $\alpha\text{-Fe(Zn)}$ layer thickness for 480 and 600 seconds annealing is however higher than the measured mean values by $2.0 \mu\text{m}$, as shown in Figure 8(d). Experimental data show, however, that about $2.0 \mu\text{m}$ oxide formed during 240 to 600 seconds annealing, which is not considered in the calculation. The calculated thickness should be thicker than the measured one by about $2.0 \mu\text{m}$, and therefore, the agreement between the measured and calculated results is reasonable.

To double check the above calibrated values, Table IV compares the calibrated effective diffusion coefficients to the lattice and grain boundary diffusion data reported.^[13–15] The lattice diffusion coefficient of Zn in the $\gamma\text{-Fe(Zn)}$ phase is calculated using $D_{\gamma\text{-Fe}}^{\text{Fe}} = 5.0 \times 10^{-5} \exp[-284,000/(RT)]$,^[14] which is the diffusivity of Fe in $\gamma\text{-Fe}$ with R gas constant and T temperature in Kelvin, because no experimental data for Zn lattice diffusion in the $\gamma\text{-Fe(Zn)}$ are available in the literature. The grain boundary diffusion coefficient in the $\gamma\text{-Fe(Zn)}$ substrate is also calculated using the above equation but with the activation energy assumed to be $0.6 \times 284,000 = 170,400 \text{ J mol}^{-1}$.^[16] It is shown that the calibrated effective Zn diffusion coefficients in the $\alpha\text{-Fe(Zn)}$ layer and in the $\gamma\text{-Fe(Zn)}$ substrate are in between the reported data for lattice diffusion and grain boundary diffusion.

The ratio of calibrated effective Zn diffusion coefficients in the $\alpha\text{-Fe(Zn)}$ and $\gamma\text{-Fe(Zn)}$ phases is about 44, which is bigger than the reported value (29) for carbon lattice diffusion but smaller than the reported one (165) for iron lattice diffusion, as shown in Table V. In Figure 9(d), it seems that the calculated $\alpha\text{-Fe(Zn)}$ layer thickness using $D_{\text{Zn}}^{\gamma} = 1.13 \times 10^{-13} \text{ m}^2 \text{s}^{-1}$ is even closer to the measured value than the one using $D_{\text{Zn}}^{\alpha} =$

$1.13 \times 10^{-14} \text{ m}^2 \text{s}^{-1}$. However, the ratio of $D_{\text{Zn}}^{\alpha}/D_{\text{Zn}}^{\gamma}$ ($5.00 \times 10^{-13}/1.13 \times 10^{-13} \approx 4$) becomes even lower than the ratio (29) for carbon lattice diffusion, which is unreasonable. Furthermore, the calculated Zn concentration in the $\gamma\text{-Fe(Zn)}$ substrate is much higher than the corresponding measured values. $D_{\text{Zn}}^{\gamma} = 1.13 \times 10^{-14} \text{ m}^2 \text{s}^{-1}$ is therefore taken as the effective diffusion coefficient in the $\gamma\text{-Fe(Zn)}$ substrate, considering the fact that the oxidation of about $2.0 \mu\text{m}$ $\alpha\text{-Fe(Zn)}$ coating is not modeled.

B. The Role of Grain Boundaries in $\alpha\text{-Fe(Zn)}$ and $\gamma\text{-Fe(Zn)}$ on Diffusion

The characteristics of the diffusion type of Zn in the $\alpha\text{-Fe(Zn)}$ coating layer and in the $\gamma\text{-Fe(Zn)}$ substrate can be determined by comparing the lattice diffusion distance to the mean grain size and grain boundary thickness $\delta \approx 5.0 \times 10^{-10} \text{ m}$ in each of these two phases. When the lattice diffusion distance is significantly smaller than the average grain size, the grain boundary diffusion distance can be estimated using the Whipple's solution^[17] as follows

$$\begin{aligned} \frac{C}{C_0} &= \text{erfc}\left(\frac{\eta}{2}\right) + \frac{\eta}{2\sqrt{\pi}} \int_1^{\Delta} \left\{ \sigma^{-3/2} \exp\left(-\frac{\eta^2}{4\sigma}\right) \text{erfc}\left[\frac{1}{2}\sqrt{\frac{\Delta-1}{\Delta-\sigma}}\left(\xi + \frac{\sigma-1}{\beta}\right)\right] \right\} d\sigma \\ \Delta &= D_{\text{gb}}/D_{\text{L}} \\ \eta &= \frac{y}{\sqrt{D_{\text{L}}t}} \\ \xi &= \frac{x-\delta/2}{\sqrt{D_{\text{L}}t}} \\ \beta &= \frac{(\Delta-1)\delta}{2\sqrt{D_{\text{L}}t}}, \end{aligned} \quad [3]$$

where C/C_0 is normalized concentration, D_{gb} and D_{L} are grain boundary and lattice diffusivities, δ is grain boundary thickness, t is diffusion time, x and y are space coordinates. Figure 10(a) shows the geometry used in the Whipple's solution: one grain boundary with two neighboring grains. The normalized concentration profile (C/C_0) along the grain boundary ($x = 0$) is numerically calculated and plotted in the $\eta - \beta$ diagram shown in Figure 10(b). The calculated lattice diffusion distance $\sqrt{D_{\text{L}}t}$ and grain boundary diffusion parameter β are shown in Table VI.

In the $\alpha\text{-Fe(Zn)}$ coating layer, the lattice diffusion distance ($1.6 \mu\text{m} < \sqrt{D_{\text{L}}t} < 2.6 \mu\text{m}$) is slightly smaller than the measured mean grain size (about $10 \mu\text{m}$ —see Table I), but they are in the same magnitude order. The grain boundary diffusion parameter ($1.8 < \beta < 2.9$) is also relatively small. Above results indicate that in the coating layer, Zn diffusion after 240 to 600 seconds annealing is Type AB and very close to Type A (bulk diffusion). Grain boundaries therefore play a certain role for diffusion, but the role is not substantial. The

Whipple's solution is therefore not suitable for calculating the diffusion distance in this phase. In the γ -Fe(Zn) substrate, the lattice diffusion distance ($0.05 \mu\text{m} < \sqrt{D_L t} < 0.09 \mu\text{m}$) is much smaller than the measured mean grain size (about $9 \mu\text{m}$), but apparently bigger than the typical grain boundary thickness $\delta \approx 5.0 \times 10^{-10} \text{ m}$. The grain boundary diffusion parameter ($340 < \beta < 550$) is relatively large. These results indicate that in this phase, Zn diffusion after 240 to 600 seconds annealing is Type B, which is in between a bulk diffusion and a grain boundary diffusion. The Whipple's solution can be used to estimate the diffusion distance of Zn along γ -Fe(Zn) grain boundaries. Let us take the annealing at 1173 K (900 °C) for 600 seconds as an example: estimated grain boundary diffusion parameter is $\beta = (\Delta - 1)\delta/(2\sqrt{D_L t}) = (1.29 \times 10^{-12}/1.13 \times 10^{-17} - 1) \times 5.0 \times 10^{-10} / (2 \times \sqrt{1.13 \times 10^{-17} \times 600}) \approx 347$. From Figure 10(b), we can find the corresponding value $\eta \approx 70$. Estimated grain boundary diffusion

distance across which the Zn concentration decreases from the equilibrium concentration 7.5 wt pct down to 0.075 wt pct is $y = \eta\sqrt{D_L t} \approx 70 \times \sqrt{1.13 \times 10^{-17} \times 600} \approx 5.76 \times 10^{-6} \text{ m}$. It should be noted that the Whipple's solution does not consider the moving α - γ phase interface, and thus, in the above calculated grain boundary diffusion, distance ($6 \mu\text{m}$) for 600 seconds annealing is over-estimated.

C. Zn Diffusion from the α -Fe(Zn) Coating into the γ -Fe(Zn) Substrate

The effect of D_{Zn}^{γ} on the calculated Zn content profiles in the γ -Fe(Zn) substrate, as shown in Figures 9(a) through (c), indicates that Zn concentration increases with D_{Zn}^{γ} with good agreement between calculations and measurements observed when $D_{Zn}^{\gamma} = 1.13 \times 10^{-14} \text{ m}^2 \text{ s}^{-1}$ (see Figures 8(a) through (c)). Comparing to the measured Zn contents, it is found that $D_{Zn}^{\gamma} = 1.13 \times 10^{-17} \text{ m}^2 \text{ s}^{-1}$ is too low and $D_{Zn}^{\gamma} = 1.13 \times 10^{-13} \text{ m}^2 \text{ s}^{-1}$ is too large. The agreement in the calculated and measured Zn concentrations in the γ -Fe(Zn) substrate (Figure 8) suggests that the 1D FDM can be used to estimate the leaking of Zn into the bulk γ -Fe(Zn) substrate from α -Fe(Zn) coating: $1.3 \mu\text{m}$ for 300 seconds annealing, $2.6 \mu\text{m}$ for 480 seconds, and $3.3 \mu\text{m}$ for 600 seconds in terms of diffusion distance. The diffusion in this phase is Type B, as discussed previously. The grain boundary diffusion distance is longer, i.e., about $6 \mu\text{m}$ estimated for 600 seconds at 1173 K (900 °C) using the Whipple's solution.

Table VI. Lattice Diffusion Distance $\sqrt{D_L t}$ and Grain Boundary Diffusion Parameter $\beta = (\Delta - 1)\delta/(2\sqrt{D_L t})$ in the α -Fe(Zn) Coating Layer and the γ -Fe(Zn) Substrate with D_L and D_{gb} Taken from Table IV

1173 K (900 °C)	240 s	300 s	480 s	600 s
α -Fe(Zn)				
$\sqrt{D_L t}$ (μm)	1.63	1.82	2.31	2.58
β	2.87	2.57	2.03	1.82
γ -Fe(Zn)				
$\sqrt{D_L t}$ (μm)	0.052	0.058	0.074	0.082
β	548	490	388	347

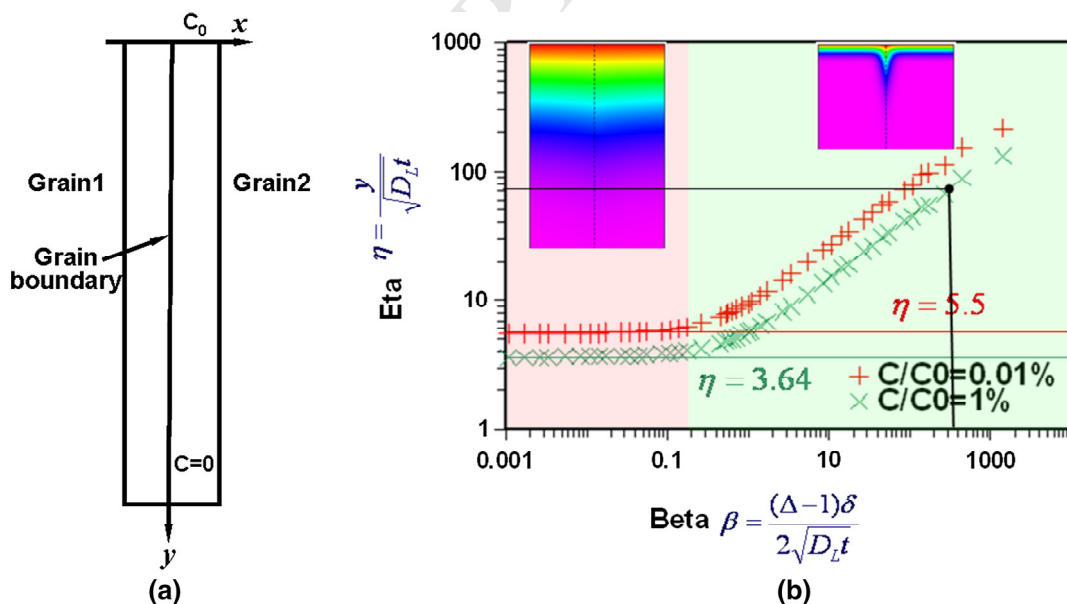


Fig. 10—(a) Grain boundary geometry used in the Whipple's solution and (b) Whipple's solution plotted using parameters Beta and Eta with $\beta = (\Delta - 1)\delta/(2\sqrt{D_L t})$ and $\eta = y/\sqrt{D_L t}$. Here, $\Delta = D_{gb}/D_L$, $\delta \approx 5.0 \times 10^{-10} \text{ m}$ and y is coordinate along grain boundary. Inserted concentration maps indicate the effect of grain boundaries on diffusion.

551 D. Micro-cracks in Side-Wall and the Role of Zn
 552 In our previous work,^[12] it has been reported that
 553 with extended duration of annealing, the depth of crack
 554 penetration into the substrate in the drawn side-wall is
 555 reduced from a maximum depth 50 μm for 240 seconds
 556 to a maximum value less than 15 μm for 600 seconds. In
 557 the undeformed top wall and in the inside side-wall (not
 558 exposed to friction forces during forming), coating
 559 cracks not penetrating the substrate were observed;
 560 however, the amount of cracks per 1 mm was independent
 561 on the duration of annealing in all sample
 562 locations. Appearance of micro-cracking at short and
 563 at long annealing times is shown in Figures 11(a) and
 564 (b). Since no liquid Zn is present even at the shortest
 565 annealing time (240 seconds), all micro-cracks are
 566 believed to be associated with friction forces during
 567 drawing. Kim *et al.*^[3] also observed rapid decrease of the
 568 depth of micro-cracks with extended annealing and
 569 assumed that progressing internal oxidation of the
 570 coating is one of the major causes reducing the crack
 571 depth due to an increase in the number of cracks in the
 572 coating layer with increasing annealing time; the stress
 573 concentrations at the crack tips during forming are
 574 therefore reduced, and the cracks are more frequent and
 575 less deep.^[3] Schwinghammer *et al.*^[18] observed that with
 576 extended time of annealing and with reduced forming
 577 temperature [as low as 1048 K (775 °C)], the micro-
 578 cracks are more frequent and less extended in depth into
 579 the substrate. However, no mechanism of cracking has
 580 been discussed apart from concluding that the
 581 micro-cracking at these conditions is clearly not related
 582 to LMIE. Drillet *et al.*^[4] found some ferritic and bainitic
 583 phases in the layer just below the coating, suggesting
 584 that severe deformation in this location induces a shift in
 585 the critical cooling rate required for martensitic trans-
 586 formation, the ferrite and bainite are stabilized and act
 587 as soft zones promoting the micro-crack propagation.
 588 When the layer is thin, the propagation is limited. Only
 589 Hensen *et al.*^[9] linked the reduced depth of micro-crack-
 590 ing with diffusion of Zn away from the grain boundaries
 591 in the coating and in the substrate. No satisfactory

reason behind the reported decrease of the micro-crack
 depth has been however provided and as can be seen
 there is no agreement on the mechanism of the
 micro-cracking and the role of extended annealing.

Based on the results presented in our previous
 contribution^[12] and in this work, we can confirm that
 there is significant change in the average concentration
 of Zn in the $\alpha\text{-Fe(Zn)}$ layer (Table II); homogenization
 of enriched Zn on grain boundaries and in pockets of
 the $\alpha\text{-Fe(Zn)}$ layer (Figure 5) occurs; $\alpha\text{-Fe(Zn)}$ layer
 grows notably (Figure 8(d)), but only insignificant
 diffusion of Zn into $\gamma\text{-Fe(Zn)}$ or across the $\alpha\text{-Fe(Zn)}/$
 $\gamma\text{-Fe(Zn)}$ interface is observed (Figures 7 and 8). Mor-
 phology of micro-cracks changes from a sharp V-shape
 type at short annealing time (240 seconds) to
 shallow and blunt U-shape type at longest annealing
 time (600 seconds) (Figure 11(b)). Relationship between
 micro-crack depth and Zn diffusion is shown in
 Figure 11(c). Interestingly, there is a clear correlation
 between amount of Zn in $\alpha\text{-Fe(Zn)}$ and the maximum
 depth of micro-crack penetration into the substrate.
 However, the bulk and grain boundary diffusion dis-
 tances of Zn into the $\gamma\text{-Fe(Zn)}$ from the $\alpha\text{-Fe(Zn)}$
 coating are slightly increasing with increasing annealing
 time, which is contrary to what would be expected if Zn
 present in $\gamma\text{-Fe(Zn)}$ controlled micro-crack propagation
 into the substrate. Homogenization of enriched Zn on
 grain boundaries and pockets (Figure 5) also plays an
 important role in reducing the micro-crack depth.

E. Mechanism of Micro-cracking

Clearly elimination of the liquid Zn from the coating
 does not prevent micro-cracking from penetrating the
 substrate; it is also evident that external forces such as
 friction shear stresses during drawing are required to
 enable propagation of micro-cracks into the substrate.
 The depth of micro-crack penetration appears to be
 dependent on the amount of Zn in $\alpha\text{-Fe(Zn)}$, and the
 Zn-rich pockets observed at short annealing time

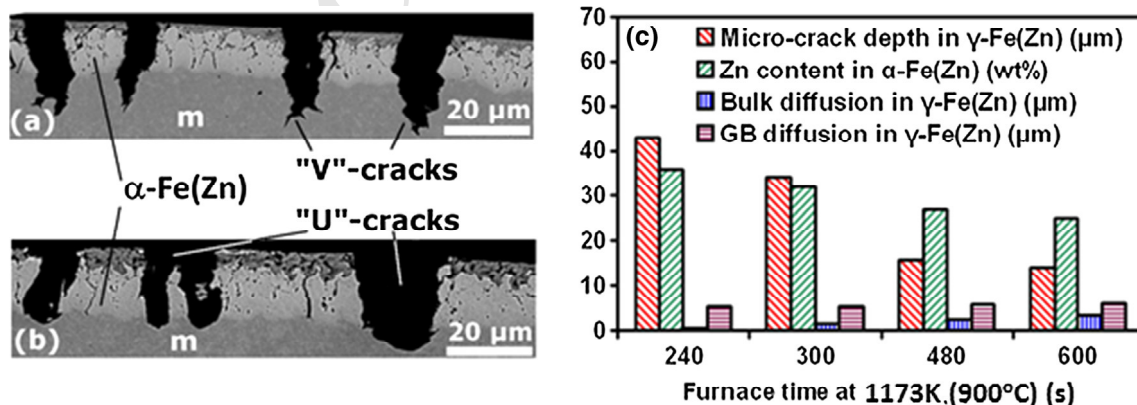


Fig. 11—Illustration of crack appearance in the drawn side-wall: (a) sharp “V”-shape of cracking penetrating deeper into the substrate (m-martensite) typical for 240 s annealing; (b) shallow and blunt “U”-spade typical after 600 s annealing; (c) Relationship between micro-crack depth and Zn diffusion in $\alpha\text{-Fe(Zn)}$ and $\gamma\text{-Fe(Zn)}$.

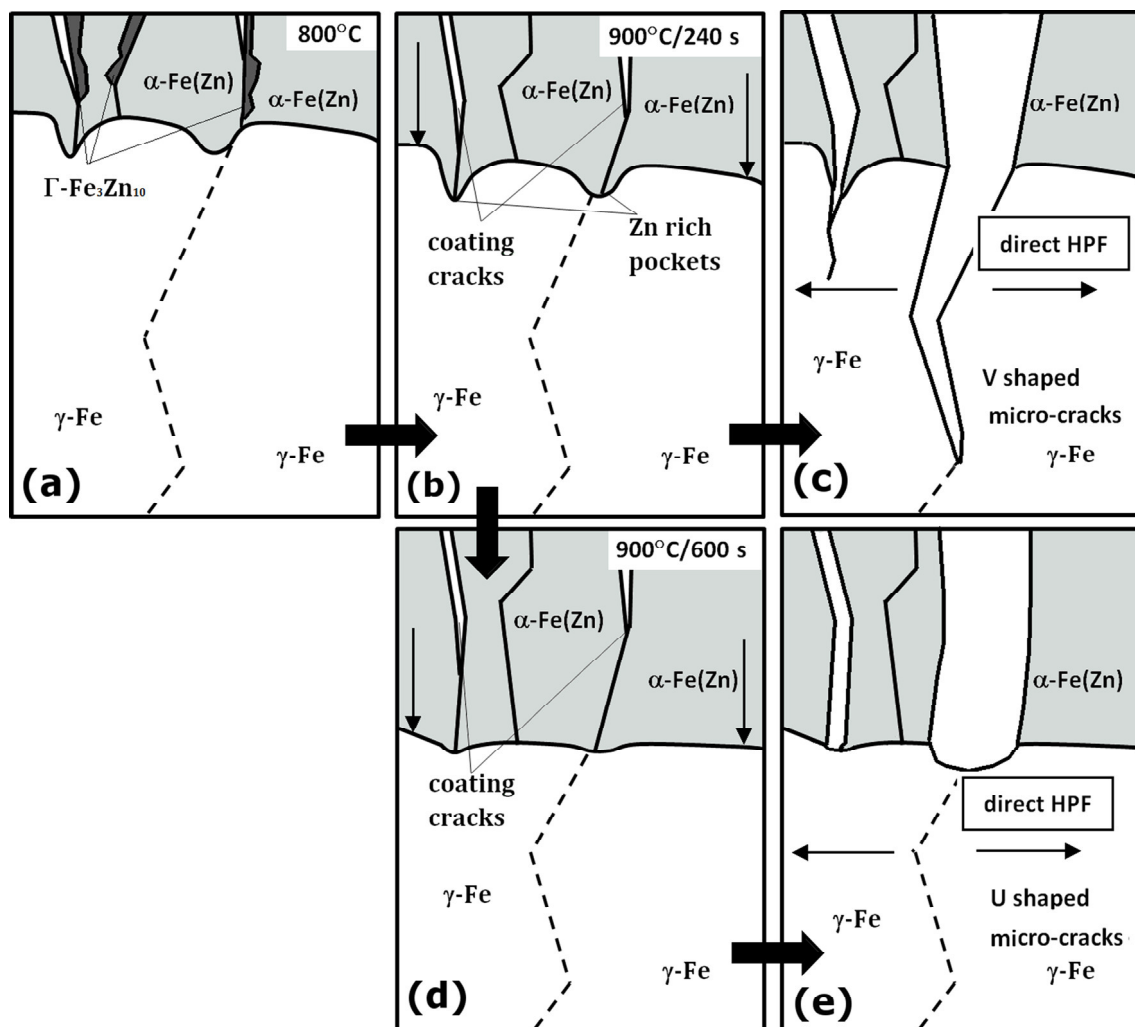


Fig. 12—Schematic Mechanism of micro-cracking of Zn-coated HPF Boron steels: (a) at 1073 K (800 °C), majority of the coating is transformed into α -Fe(Zn), in certain areas especially at α -Fe(Zn) GBs, Zn-rich phase Γ -Fe₃Zn₁₀ is present; (b) at 1173 K (900 °C) and 240 s hold Γ -Fe₃Zn₁₀ is fully transformed into α -Fe(Zn), Zn-rich pockets inside the α -Fe(Zn) coincide with previous Γ -Fe₃Zn₁₀, α -Fe(Zn) contains several coating cracks not penetrating the substrate; (c) if external load is applied during HPF, Zn-rich pockets and high Zn content on the α -Fe(Zn) side of the interface assist micro-cracking due to SMIE mechanism, micro-cracks are up to 50 μ m deep and have a sharp V shape; (d) if holding at 1173 K (900 °C) is extended to 600 s α -Fe(Zn) layer growths, Zn-rich pockets disappear and amount of Zn in the α -Fe(Zn) layer is reduced leading to a reduced availability of Zn atoms to assist SMIE; (e) cracks almost do not penetrate the substrate and have shallow and blunt U shape.

possibly enhance the micro-crack propagation. Lynch observed on notched Al-Zn-Mg-Cu alloy specimens exposed to constant external load in solid Indium environment^[19] that in the conditions where even no liquid In is present and embrittlement atoms are transferred from solid In phase, the solid-metal-induced embrittlement (SMIE) leading to inter-granular cracking is active. The crack velocity during SMIE^[20] is lower than in LMIE, and higher external stresses to propagate SMIE crack are required, and if the external stress is below a threshold value, no SMIE will occur.^[19] Gordon proposed^[21] that transport of the embrittlement atoms in the solid state toward the crack tip consists of a surface self-diffusion of embrittler atoms over a layer of adsorbed embrittler atoms thick enough to allow self-diffusion. Lynch accepted this mechanism and in his later works on various materials under LMIE and

SMIE^[22–24] suggested that embrittling adsorbed atoms induce dislocation emission from the crack tip leading to increased localized slip.

In our work, we have not detected any Zn present on the surface of the cracks but we cannot exclude that (only) several Zn atoms thick surface layer may be present during initial crack extension into the γ -Fe(Zn) (γ -Fe(Zn) is transformed to martensite during die quenching), and this thin surface Zn layer could be either oxidized or further mechanically cracked during HPF. Our proposed mechanism of micro-cracking of Zn-coated HPF B steels is shown in Figure 12: (a) at 1073 K (800 °C), majority of the coating is transformed into α -Fe(Zn), in certain areas especially at α -Fe(Zn) grain boundaries, Zn-rich phase Γ -Fe₃Zn₁₀ is present; (b) at 1173 K (900 °C) and 240 seconds hold any remaining Γ -Fe₃Zn₁₀ is fully transformed into α -Fe(Zn),

Zn-rich pockets inside the α -Fe(Zn) coincide with previous Γ -Fe₃Zn₁₀, α -Fe(Zn) contains several coating cracks not penetrating the substrate; (c) if external load is applied during HPF Zn-rich pockets and high Zn content on the α -Fe(Zn) side of the interface assist micro-cracking due to SMIE mechanism, micro-cracks are up to 50 μ m deep and have a sharp V shape; (d) if holding at 1173 K (900 °C) is extended to 600 seconds α -Fe(Zn) layer growths, homogenization of Zn-enriched areas on α -Fe(Zn) grain boundaries and of Zn-rich pockets takes place as well as the reduction of concentration of Zn in the α -Fe(Zn) layer, that all lead to a reduced availability of Zn atoms to assist SMIE; (e) when external load during HPF is applied, micro-cracks almost do not penetrate the substrate and have shallow and blunt U-shape; external tensile loads probably just open the pre-existing thermal coating cracks and plastically deform them. SMIE is not active due to low availability of solid Zn atoms in the α -Fe(Zn).

V. CONCLUSIONS

In this study, a combination of experimental and simulation work has been carried out to link Zn distribution changes in Zn-coated 22MnB5 annealed at 1173 K (900 °C) with micro-cracking occurring during HPF. The main conclusions of this study are summarized as follows:

1. The thickness of α -Fe(Zn) coating increases with annealing time from 18 to 22 μ m after 300 to 600 seconds of annealing, this is accompanied by a Zn concentration decrease in the α -Fe(Zn) coating and a Zn concentration increase in the γ -Fe(Zn) substrate.
2. The thickness of α -Fe(Zn) coating is controlled by the Zn diffusion coefficients both in the α -Fe(Zn) phase and in the γ -Fe(Zn) phase. Effective diffusion coefficient of Zn is $5.00 \times 10^{-13} \text{ m}^2 \text{ s}^{-1}$ in the α -Fe(Zn) and $1.13 \times 10^{-14} \text{ m}^2 \text{ s}^{-1}$ in the γ -Fe(Zn) substrate.
3. Bulk Zn diffusion distance in the γ -Fe(Zn) substrate increases from 1.3 μ m after 240 seconds annealing to 3.3 μ m after 600 seconds annealing at 1173 K (900 °C), Zn grain boundary diffusion distance in the γ -Fe(Zn) substrate after 600 seconds is 6 μ m. Zn diffusion in the α -Fe(Zn) coating layer is Type AB and very close to Type A (bulk diffusion), the diffusion in the γ -Fe(Zn) substrate is Type B (between bulk diffusion and grain boundary diffusion).
4. The Zn diffusion during annealing is not the only responsible factor for the formation of micro-cracks that have a maximum depth of 15 to 50 μ m, exceeding maximum diffusion distance of 6 μ m. Reduced amount of Zn-rich pockets at α -Fe(Zn) grain boundaries, together with reduced Zn concentration in α -Fe(Zn) with increasing annealing time contribute to the reduced susceptibility to deep micro-cracks in the samples annealed for longer

time (480 seconds and 600 seconds). SMIE is likely to be active during short times of annealing when enriched Zn is present on α -Fe(Zn) grain boundaries and in the pockets where mean Zn content is relatively high, and SMIE is therefore responsible for the deep V-shape cracks. Zn in α -Fe(Zn) is homogenized and mean Zn concentration is lowered in the α -Fe(Zn) coating after long time annealing, thus no SMIE is active due to lower availability of solid Zn atoms in the α -Fe(Zn), and the blunt U-shape cracks are due to external loads only.

ACKNOWLEDGMENTS


The financial assistance from the WMG Centre High Value Manufacturing Catapult with focus on low C mobility and Tata Steel is gratefully acknowledged. The authors are thankful for the assistance from Dr. Richard Beanland and Steven Hindmarsh at MAS, University of Warwick with the TEM analysis with FIB lift-out. The authors also wish to thank Dr Didier Farrugia for discussing aspects of the diffusion modeling.

REFERENCES

1. European Automotive Research Partners Association R&D technology Roadmap, http://www.earpa.eu/docs/2005/furore_road_map_final.pdf.
2. T. Altan: *Stamp. J.*, 2011, vol. 19, p. 10.
3. S. Kim, I. Son, D. Kim, and S. Kim: *4th Int. Conf. on Hot Sheet Met. Forming of UHSS*, Lulea, 2013.
4. P. Drillet, R. Grigorieva, G. Leuillier, and T. Vietoris: *Study of Cracks Propagation Inside the Steel on Press Hardened Steel Zinc Based Coatings*, 2011, Galvatech, Genova.
5. M.J. van Genderen, W. Verloop, J. Loiseaux, and G. Hensen: *3rd Int. Conf. on Hot Sheet Met. Forming of UHSS*, Kassel, 2011.
6. C.W. Lee, D.W. Fan, I.R. Sohn, S.J. Lee, and B.C. De Cooman: *Metall. Mater. Trans. A*, 2012, vol. 43, pp. 5122–27.
7. L. Cho, H. Kang, C. Lee, and B.C. De Cooman: *Scripta Mater.*, 2014, vols. 90–91, pp. 25–28.
8. T. Kurz, G. Luckeneder, T. Manzenreiter, and H. Schwinghammer: *Zinc Coated Press-Hardening Steel—Challenges and Solutions*, SAE Technical Paper 2015-01-0565, 2015.
9. G. Hensen, W. Melfo, and S.P. Chen: *4th Int. Conf. on Hot Sheet Met. Forming of UHSS*, Lulea, 2013.
10. A.R. Marder: *Prog. Mater. Sci.*, 2000, vol. 45, pp. 199–271.
11. R. Autengruber, G. Luckeneder, S. Kolnberger, J. Faderl, and A.W. Hassel: *Steel Res. Int.*, 2012, vol. 83, pp. 1005–11.
12. V. Janik, P. Beentjes, D. Norman, G. Hensen, and S. Seetharaman: *Proceedings of MST2014 Conference*, Pittsburgh, 2014.
13. I. Richter and M. Feller-Kniepmeier: *Phys. Status Solidi A*, 1981, vol. 68, pp. 289–300.
14. E.A. Brandes and G.B. Brook, eds.: *Smithells Metals Reference Book*, 7th ed., Butterworth & Heinemann, Oxford, 1992.
15. J.S. Dohie, J.R. Cahoon, and W.F. Caley: *JPEDAV*, 2007, vol. 28, pp. 322–27.
16. P. Heitjans and J. Karger, eds.: *Diffusion in Condensed Matter: Methods, Materials, Models*, 2nd ed., Birkhauser, Boston, 2005.
17. R.T.P. Whipple: *Philos Mag.*, 1954, vol. 45, p. 1225.
18. H. Schwinghammer, G. Luckeneder, T. Manzenreiter, M. Rosner, P. Tsipouridis, and T. Kurz: *4th Int. Conf. on Hot Sheet Met. Forming of UHSS*, Lulea, 2013.

784	19. S.P. Lynch: <i>Mat Sci Eng</i> , 1989, vol. A108, pp. 203–12.	788
785	20. S.P. Lynch: <i>Mater. Charact.</i> , 1992, vol. 28, pp. 279–89.	789
786	21. P. Gordon: <i>Metall. Trans.</i> , 1978, vol. 9A, pp. 267–73.	790
787	22. S.P. Lynch: <i>Acta Metall.</i> , 1988, vol. 36, pp. 2639–61.	791
	23. S.P. Lynch: in <i>Environment Induced Cracking of Materials</i> , S. Shipilov, R. Jones, J.-M. Olive, and R. Rebak, eds., Elsevier, Amsterdam, 2007, pp. 167–177.	792
	24. S.P. Lynch: <i>Metall. Trans.</i> , 2013, vol. 44A, pp. 1209–29.	

UNCORRECTED PROOF

	Journal : MMTA	Dispatch : 19-10-2015	Pages : 13
	PIPS No. : 3203	<input type="checkbox"/> LE	<input type="checkbox"/> TYPESET
	MS Code :	<input type="checkbox"/> CP	<input type="checkbox"/> DISK